Cell Motility and the Cytoskeleton (2009)

Bend Propagation in the Flagella of Migrating Human Sperm, and Its Modulation by Viscosity

D. J. Smith,[1,2,3]* E. A. Gaffney,[3,4] H. Gadêlha,[3,4,5] N. Kapur,[6] and J. C. Kirkman-Brown[1,3]

[1]*School of Clinical and Experimental Medicine, University of Birmingham, Edgbaston, Birmingham, United Kingdom*

[2]*School of Mathematics, University of Birmingham, Edgbaston, Birmingham, United Kingdom*

[3]*Centre for Human Reproductive Science, Birmingham Women's NHS Foundation Trust, Edgbaston, Birmingham, United Kingdom*

[4]*Mathematical Institute, University of Oxford, Oxford, United Kingdom*

[5]*The CAPES Foundation, Ministry of Education of Brazil, Brasilia, Brazil*

[6]*School of Mechanical Engineering, Faculty of Engineering, University of Leeds, Leeds, United Kingdom*

A pre-requisite for sexual reproduction is successful unification of the male and female gametes; in externally-fertilising echinoderms the male gamete is brought into close proximity to the female gamete through chemotaxis, the associated signalling and flagellar beat changes being elegantly characterised in several species. In the human, sperm traverse a relatively high-viscosity mucus coating the tract surfaces, there being a tantalising possible role for chemotaxis. To understand human sperm migration and guidance, studies must therefore employ similar viscous in vitro environments. High frame rate digital imaging is used for the first time to characterise the flagellar movement of migrating sperm in low and high viscosities. While qualitative features have been reported previously, we show in precise spatial and temporal detail waveform evolution along the flagellum. In low viscosity the flagellum continuously moves out of the focal plane, compromising the measurement of true curvature, nonetheless the presence of torsion can be inferred. In high viscosities curvature can be accurately determined and we show how waves propagate at approximately constant speed. Progressing waves increase in curvature approximately linearly except for a sharper increase over a distance $\sim$20–27 μm from the head/midpiece junction. Curvature modulation, likely influenced by the outer dense fibres, creates the characteristic waveforms of

Additional Supporting Information may be found in the online version of this article.

Contract grant sponsor: MRC Special Training Fellowship; Contract grant number: G0600178; Contract grant sponsor: CAPES Foundation; Contract grant number: BEX-4676/06-8; Contract grant sponsors: Hester Cordelia Parsons Fund, Wellcome Trust, MRC.

*Correspondence to: D. J. Smith, School of Mathematics, University of Birmingham, Edgbaston, Birmingham B15 2TT, United Kingdom. E-mail: d.j.smith.2@bham.ac.uk

Received 4 December 2008; Accepted 22 January 2009

Published online 00 Month 2009 in Wiley InterScience (www.interscience.wiley.com).
DOI: 10.1002/cm.20345

high viscosity swimming, with remarkably effective cell progression against greatly increased resistance, even in high viscosity liquids. Assessment of motility in physiological viscosities will be essential in future basic research, studies of chemotaxis and novel diagnostics. Cell Motil. Cytoskeleton 2009.

Key words: flagellum; human sperm; viscosity; migration; chemotaxis

INTRODUCTION

The evolution of sexual reproduction has produced numerous forms of gametes adapted to differing physical environments. Elegant research has elucidated in detail the mechanisms of sperm motility and chemotaxis in external fertilising marine animals such as sea urchins and starfish [Ward et al., 1985; Wood et al., 2003; Nishigaki et al., 2004; Bohmer et al., 2005; Shiba et al., 2005]. This work has rapidly advanced to encompass details of motility regulation by calcium signalling, cAMP, and peptides such as speract [Ohmuro et al., 2004; Shiba et al., 2005, 2006; Kinukawa et al., 2006; Wood et al., 2007]. Tantalising initial work suggests that chemotaxis and other forms of motility modulation may also be critical to human fertilisation [Spehr et al., 2003, 2006; Eisenbach and Giojalas, 2006; Teves et al., 2006; Eisenbach, 2007], but a crucial difference between marine and internal fertilisation is the viscosity of the fluid environment.

High speed imaging, often allied to fluid mechanics modelling, has long been an important tool in biophysical research on flagellar propulsion [Gray, 1953; Gray, 1955; Gray and Hancock, 1955], although in recent years it appears to have been under-exploited in biomedical research on the human male gamete. Advances in digital high-speed imaging, capture and processing, now permit highly detailed analysis of the development and propagation of the flagellar waveform and its effect on cell migration. Indeed this approach may provide a tangible way to link initial work on human sperm chemotaxis to detailed models of motility modulation via changes to the flagellar beat, in addition to offering new diagnostic and drug screening techniques, including the development of next-generation Computer-Aided Semen Analysis (CASA) technologies.

An important initial step is to develop a detailed characterisation of the development and propagation of the human sperm flagellar waveform, and how this relates to cell progression in the migrating population in liquids that approximate physiological conditions. Classic research on human sperm migrating in cervical mucus (or analogues), known as (modified) 'Kremer penetration assays' [Kremer, 1965; Katz et al., 1980; Mortimer et al., 1990; Aitken et al., 1992; Ivic et al., 2002; Ola et al., 2003] have examined the migrating subpopulation of cells, however available data have mainly concerned qualitative characterisations of the waveform [Katz et al., 1978] and quantitative statistical analysis of the effect of frequency and beat amplitude on progressive velocity in 'vanguard' and 'following' cells [Katz et al., 1978, 1982].

A number of biophysical studies have examined the relation between the crucial functional property of progressive velocity and flagellar parameters such as frequency and wavespeed, which according to fluid mechanics modelling [Dresdner and Katz, 1981], should be directly proportional. The early classic study of Gray and Hancock [1955] in sea urchin suggested that a relatively simple formula for propulsive velocity from measured flagellar parameters could give remarkable predictive power when averaged across a large sample of cells. A subsequent study of ram sperm swimming in semen [Denehy, 1975] found their formula to be less successful in this situation, and an empirical law based on frequency and beat amplitude sampled at two locations was found to be more accurate.

A resurgence of interest in the flagellar movement of other mammalian species' sperm in the last decade has led to a number of important discoveries. Digital image capture and analysis has revealed that in progressively motile cells, the flagellar beat parameters of wavelength and frequency vary dependently, unlike in marine species [Ishijima et al., 2002, 2006; Ohmuro and Ishijima, 2006], and that the hyperactivated state of rodent sperm, a prerequisite to penetration of the oocyte vestments [Suarez and Ho, 2003], involves a change from constant-curvature to constant-frequency beating [Ohmuro and Ishijima, 2006; Kaneko et al., 2007].

These studies have generally employed low viscosity liquids for cell imaging, however, physiological liquids and analogues differ from low viscosity media by virtue of both high viscosity and non-Newtonian rheology. Some studies have examined the effect of polymer-containing media on progressive velocity of human sperm [Katz et al., 1978; Katz and Berger, 1980; Dresdner and Katz, 1981; Ishijima et al., 1986], and the effect on straightness of progression on hyperactivated mouse sperm cells [Suarez and Dai, 1992]. Two important studies in the human [Katz et al., 1978; Katz and Berger,

1980] have suggested a weak positive correlation between frequency and progressive velocity, and between amplitude and progressive velocity, when examining very heterogeneous populations in experiments where cells were not required to migrate significant distances. A Kremer assay study of migrating cells [Katz et al., 1982] suggested that progressive velocity is related to frequency and amplitude through power laws, and that these laws change with the disruption of the mucus microstructure by the migrating population, although detailed sample statistics were not given. The biophysics underlying flagellar propulsion in physiological liquids are therefore likely to be very complex, and detailed initial data on the flagellar beat is essential for researchers developing such models.

We shall focus on precise measurement and characterisation of the flagellar waveform and kinematic parameters of migrating human sperm cells in a standardisable analogue liquid that has been shown to be an excellent simulant of cervical mucus [Ivic et al., 2002], selecting cells for imaging with a sperm penetration assay, an excellent predictor of in vitro fertilisation [Barratt et al., 1989]. For the first time we characterise how the curvature wave propagates and changes along the flagellum in such cells, and discuss the relative advantages and disadvantages of low and high viscosity media for the assessment of flagellar movement and sperm motility in biomedical and clinical assays.

MATERIALS AND METHODS

Sperm Penetration Medium

Low viscosity penetration medium was based on supplemented Earle's Balanced Salt Solution without phenol red, containing energy substrates 5 mM glucose, 2.5 mM Na pyruvate and 19 mM Na lactate (041-94189H, Gibco-BRL, Paisley, UK), with 0.45% human serum albumin (BioProducts Laboratory, Elstree, UK) added to prevent cells from adhering to the inner glass surfaces of the capillary tubes. High viscosity medium was produced by adding 1% methylcellulose (M0512, Sigma-Aldrich, Poole, UK, specified so that an aqueous 2% solution gives a nominal viscosity of 4000 centipoise or 4 Pa·s at 20°C), and very high viscosity medium was produced by adding 2% methlycellulose solution.

Selection of the Migrating Population

Penetration medium was loaded by capillary action into flat-sided borosilicate capillary tubes (*VITROTUBES*, 2540, Composite Metal Services, Ilkley, UK) with length 50 mm, and inner dimensions 4 mm × 0.4 mm. One end of the tube was sealed with *CRISTASEAL* (Hawksley, Sussex, UK, #01503-00). Cells were selected for imaging by immersing one end of the capillary tube into a *BEEM* capsule (G360-2, size 00, Agar Scientific, Stansted, UK) containing a 200 μl aliquot of raw semen, prepared using a positive-displacement pipette, within 15 min of sample production. Incubation was performed for 30 min at 37°C in 6% CO_2.

Imaging

Cells were imaged at ~2 cm migration distance into the capillary tube, and all cells analysed statistically were imaged in the 'surface accumulated' layer 10–20 μm from the inner surface of the capillary tube. Imaging was performed with an Olympus (BX-50) microscope, using a positive phase contrast lens (20×/0.40 ∞/0.17 Ph1, depth of field ~5.8 μm) together with a Hamamatsu Photonics C9300 CCD camera at 293–332 frames per second, streaming data directly to a Dell Dimension 64 bit Workstation, running Wasabi software (Hamamatsu). The stage was maintained at 37°C using a LINKAM C0102 stage heater. The C9300 CCD sensor resolution is 640 × 480 with pixel size 7.4 × 7.4 μm, although imaging was performed with sub-arraying without binning to ~640 × 200 to achieve the necessary frame-rate.

Image Analysis

Flagellar movement analysis was performed using custom thresholding macros in Image Pro Plus (Media-Cybernetics) to extract the flagellum position, and post-processing and analysis was performed in MATLAB (Mathworks) with the Image Processing, Spline and Curve Fitting Toolboxes. Data smoothing routines using the MATLAB 'csaps' function were used to remedy random loss of the distal flagellum, and additionally to remove spatial and temporal noise in the extracted flagellum position. The smoothed data were compared post-hoc with the original data to ensure that the smoothing routines did not cause significant deviations from the original data.

It has previously been established [Phillips, 1972] that the human sperm head rolls as the cell progresses rather than simply rocking back-and-forth, and this has also been confirmed with double-focal microscopy [Ishijima et al., 1992]. The cell rolling rate was captured by using thresholding to capture the white region in the head, then using the Image Pro Plus tracking function with the 'roundness' parameter. This parameter takes value 1.00 for a perfect circle and is greater than 1 for more elongated objects, so that the broad face of the cell is indicated by a value of ~1.05 and the narrow face by a value of ~1.25. This measure was found to be more robust to noise than the visible head width.

While rolling and flagellar beat frequencies could be measured directly from images, the model of Rikmenspoel [1965] formulated for bull sperm was also

used in the following form to 'predict' rolling frequency and beat frequency from the peak frequencies evident in the flagellar power spectra:

$$\text{Rolling frequency} = (\text{second peak frequency} - \text{first peak frequency})/2, \quad (1)$$

$$\text{Beat frequency} = (\text{second peak frequency} + \text{first peak frequency})/2. \quad (2)$$

The 'predicted' values are compared with the observed values in Results, Fig. 4, in order to test the assumption of constant head rolling rate underlying the model.

Progressive velocity was determined directly from the distance moved by the head/neck junction over the entire imaging period, which over several beat cycles converges very rapidly to the equivalent CASA (Computer Aided Semen Analysis) parameter '*VSL*'. Wavelength and wavespeed were determined with respect to distance along the curved flagellum axis rather than straight line distance from the head, termed 'arclength'.

Results for a total of 36 cells are given, 16 in low viscosity liquid, 19 in high viscosity liquid, and 1 in very high viscosity liquid.

Semen Samples

Semen samples were obtained from normozoospermic research donors giving informed consent at the Centre for Human Reproductive Science, Birmingham Women's NHS Foundation Trust by masturbation, after 2–4 days' abstinence. Imaging and analysis was performed on cells from at least 10 donors; data shown in this study were taken from four representative donors.

Rheometry

Rheometry measurements were performed at 37°C using a Bohlin CVO120 HR cone-and-plate rheometer in oscillatory mode with a 60 mm, 1° cone.

RESULTS

Rheological Properties of Sperm Penetration Media

We report the values of storage modulus G' and shear modulus G'' at 5 Hz, for comparison with the midcycle mucus values given by [Wolf et al., 1977]. This early study reported G' and G'' both $\sim$30 dyn/cm^2 (3 Pa) at an angular frequency of 30 rad/s (4.8 Hz), at 'Day 0' of the menstrual cycle. Fitting a Maxwell model to these values – see for example [Smith et al., 2007] – gives estimates of relaxation time 0.033 s and effective viscosity 0.2 Pa·s. These values vary significantly between samples, as indicated by the wide confidence intervals on the graph, but give an order-of-magnitude estimate for the rheological properties of midcycle mucus. At Day 5, the values reported ($G' = 10$ Pa, $G'' = 12$ Pa) suggest a similar effective relaxation time (0.027 s) but a much larger effective viscosity (0.680 Pa·s), the confidence interval indicating up to two-fold variation in viscosity between samples.

High viscosity medium was found to have $G' = 0.76$ Pa and $G'' = 4.16$ Pa at 31 rad/s (5 Hz), from which we estimate a relaxation time of 0.006 s and an effective viscosity 0.14 Pa·s. High viscosity medium therefore has similar magnitude viscosity to midcycle mucus, but is less elastic.

Very high viscosity medium was found to have $G' = 20.8$ Pa and $G'' = 39.2$ Pa, from which we estimate relaxation time 0.017 s and viscosity 1.6 Pa·s. The viscosity is slightly greater than the upper confidence limits reported previously [Wolf et al., 1977], while the relaxation time is of a similar order of magnitude.

Flagellar Movement and Progression of Cells Migrating in Low and High Viscosity Media

Figures 1a–1c show progressive velocity versus various flagellar wave kinematic parameters, for cells in low viscosity medium (blue) and high viscosity medium (red) at 37°C. In low viscosity medium, mean values across 16 cells in the migrating population were progressive velocity 62 μm/s, progression per beat 2.7 μm, frequency 23 Hz, wavelength 39 μm, wavespeed 890 μm/s. In high viscosity medium, mean values across 19 cells in the migrating population were progressive velocity 65 μm/s, progression per beat 5.8 μm, frequency 11 Hz, wavelength 18 μm, wavespeed 200 μm/s (all data given to two significant figures).

In low viscosity, the strongest correlation ($R^2 = 0.60$, $n = 16$, $P < 0.0001$) is found between wavespeed and progressive velocity, with weaker but significant correlations ($R^2 = 0.39$ and 0.22, respectively, $n = 16$, $P < 0.01$) for wavelength and beat frequency. In high viscosity liquid, all correlations were found to be very weak ($R^2 = 0.041$, 0.014, and 0.0003, for wavespeed, wavelength and beat frequency respectively, $n = 19$, not statistically significant).

Progression per beat, also referred to as 'progressive kinetic efficiency' [Katz et al., 1978] was found to be correlated to wavelength in both media (Fig. 1d, $R^2 = 0.57$ and 0.44, respectively, $P < 0.001$).

Subsequent findings are given for individual cells, however all findings were found to be representative of the populations studied in low and high viscosity liquid. The cell shown in detail in low viscosity medium had progressive velocity 62 μm/s, progression per beat 2.7 μm, frequency 24 Hz, wavelength 39 μm, wavespeed 920 μm/s; the cell shown in detail in high viscosity

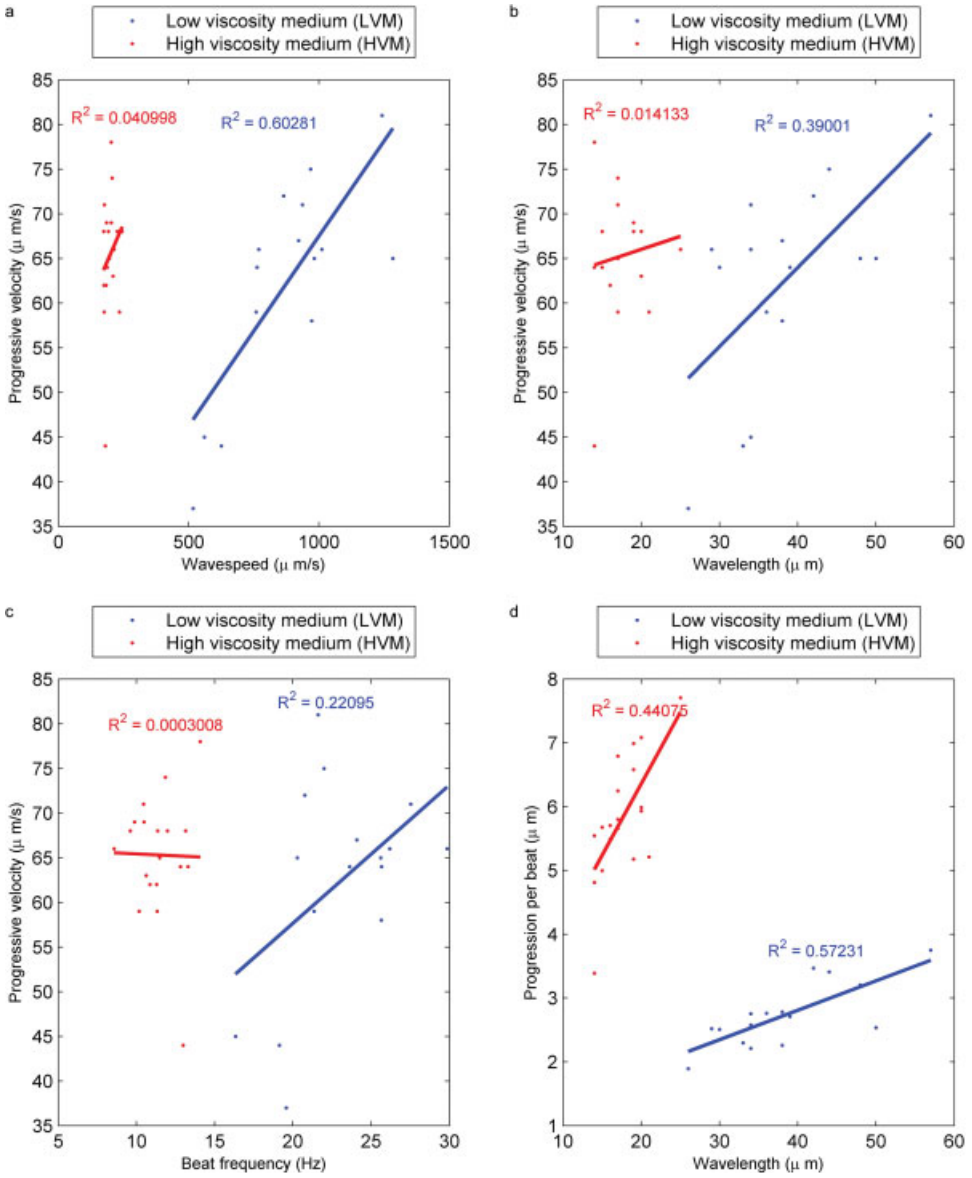

Fig. 1. (**a**–**c**) Progressive velocity and (**d**) progression per beat, versus the flagellar kinematic parameters (a) wavespeed, (b) wavelength, (c) beat frequency and (d) wavelength. Points in blue denote low viscosity, points in red denote high viscosity, lines represent linear regression fits, with R^2 values indicated. In low viscosity liquids, all correlations calculated were statistically significant whereas in high viscosity, only the correlation between wavelength and progression per beat was statistically significant.

medium had progressive velocity 58 μm/s, progression per beat 5.7 μm, frequency 10 Hz, wavelength 19 μm, wavespeed 200 μm/s.

Head Centreline Deviation

Head centreline deviation D typically exhibited a 'double-frequency' periodic behaviour (example results for a single cell at arclength 10 μm shown in Fig. 2b) for cells in low viscosity medium. In high viscosity (example results shown in Fig. 2c), we found a nearly single-frequency behaviour, although the average value of the latter plot is slightly below zero due to asymmetry of the flagellar beat.

Analysis of the Fourier power spectra of D at all arclength positions of the flagellum (example result, Fig. 7e) confirmed that cells in low viscosity exhibited two non-zero frequencies. Cells in high viscosity sometimes exhibited just one frequency peak, some had an additional 'zero frequency mode', corresponding to asymmetry of the flagellar beat, while some cells exhibited a weak low frequency mode, as evident in Fig. 9e.

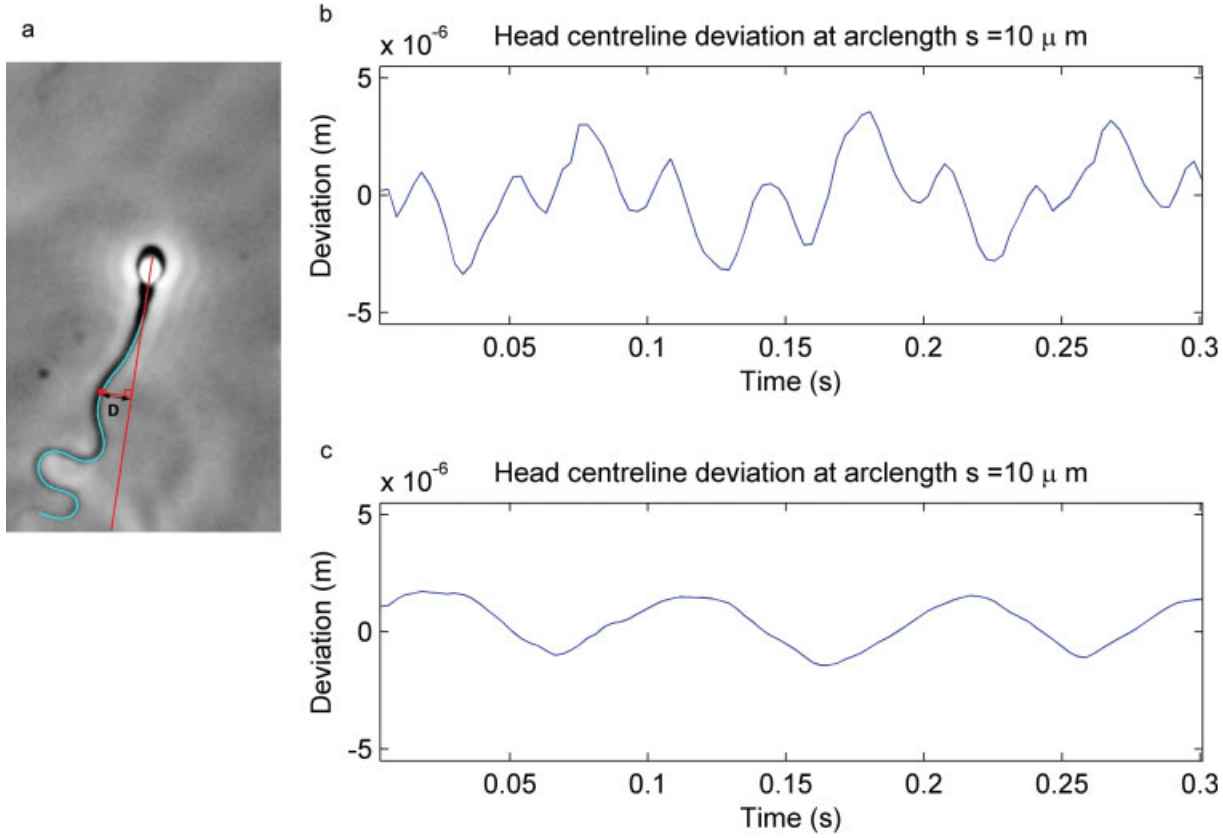

Fig. 2. The quantity 'head centreline deviation' D. (**a**) Diagram showing the calculation of D for an example high viscosity cell. (**b**) Plot of D against time at a point an arclength of 10 microns from the head, for an example cell in low viscosity liquid, analysed in detail in Fig. 7. (**c**) Plot of D against time at a point an arclength 10 microns from the head, for an example cell in high viscosity liquid, analysed in detail in Fig. 9.

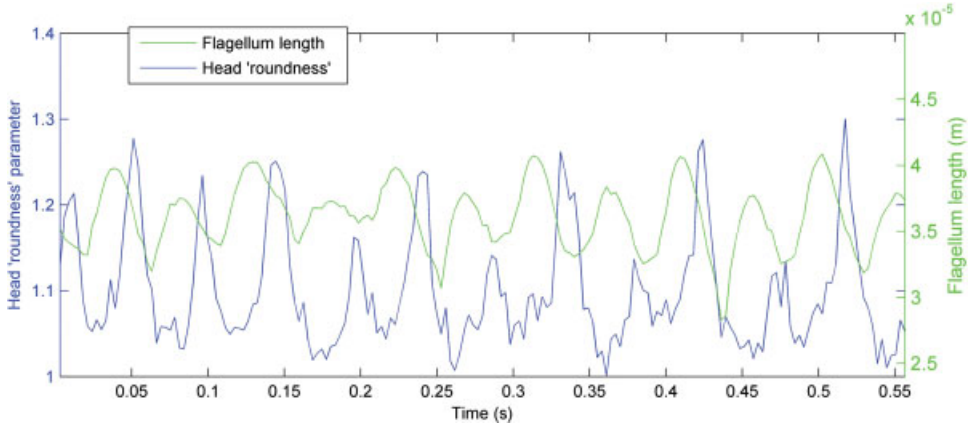

Fig. 3. Example results for head rolling and captured two-dimensional flagellum length in low viscosity liquid. Blue axis: the 'roundness' parameter calculated from the image of the sperm head, to indicate cell rolling. Green axis: the two-dimensional apparent flagellum length of the same cell, indicating the rolling of the flagellar beat three-dimensional envelope.

Cell Rolling and Out-of-Plane Movement in Low Viscosity Liquids

Figure 3 (blue axis) plots example results for the variation in 'head roundness' parameter, as described in Materials and Methods, revealing the rolling of the sperm flagellum. A value of ∼1.25 indicates that the thinner profile of the cell is visible, while a value of 1.05 indicates that the flatter profile of the cell is visible, the period between two peaks corresponding to a roll of 180°. The captured flagellum length, revealing out-of-

plane movement of the flagellum is shown on the green axis. Typically oscillations in both quantities occur at the same frequency, confirming that the head and the major plane of the flagellar beat rotate at the same rate.

Figure 4a shows the variations in cell rolling frequency with flagellar beat frequency in low viscosity liquid across a sample of cells. There is a relatively weak positive correlation ($R^2 = 0.21$, $n = 16$). The mean rolling rate was 11.2 Hz (range 6.9–14.7 Hz, standard deviation 2.5 Hz), the mean flagellar beat frequency was 23.1 Hz (range 16.3–29.8 Hz, standard deviation 3.6 Hz). Figures 4b and 4c show the correlation between observed frequencies and predicted frequencies based on the formula of Rikmenspoel (Eqs. 1 and 2, Materials and Methods). The match for roll frequency is relatively poor, although the positive correlation is statistically significant ($R^2 = 0.45$, $P = 0.0022$). For flagellar beat frequency is the match is relatively good (mean error ~8%), and the correlation is again highly significant ($R^2 = 0.80$, $P < 0.0001$).

Cell Rolling and Flagellar Planarity in High Viscosity Liquid

A combination of non-rolling and rolling cells was observed in high viscosity liquid, respective examples being shown in Figs. 5 and 6. Non-rolling cells always presented the flat side of the head to the viewer, likely due to the constraining effect of the nearby surface. In non-rolling cells, continuous acquisition of the waveform without the introduction of rolling artefacts is possible with conventional two-dimensional monochrome imaging. Among rolling cells the flagellar waveform appeared to be approximately planar, judged from the appearance of the waveform when the thin edge of the cell head presented (Figs. 6a and 6c). We did not attempt to capture or analyse the flagellar wave quantitatively as it rolled onto its side. Similar results were evident in very high viscosity liquid. Rolling cells in high viscosity exhibited a typical rolling rate of ~1.5 Hz.

Analysis of the Flagellar Waveform: Low Viscosity Liquid

Figure 7 shows various detailed measures of the flagellar movement of a representative cell in low viscosity liquid, with Fig. 7a showing an example imaging frame, with the captured flagellum as a cyan line; see also Supporting Information Fig. 1 and Movie 1. The trajectory of the proximal end of the flagellum (b, green trace), equivalent to a high-resolution computer-aided semen analysis track, shows the complex but near-periodic nature of the cell trajectory in low viscosity, in addition to the significant yawing of the head. The curvature portrait (c) shows the captured two-dimensional bending wave as it progresses. Red/yellow indicates curvature in

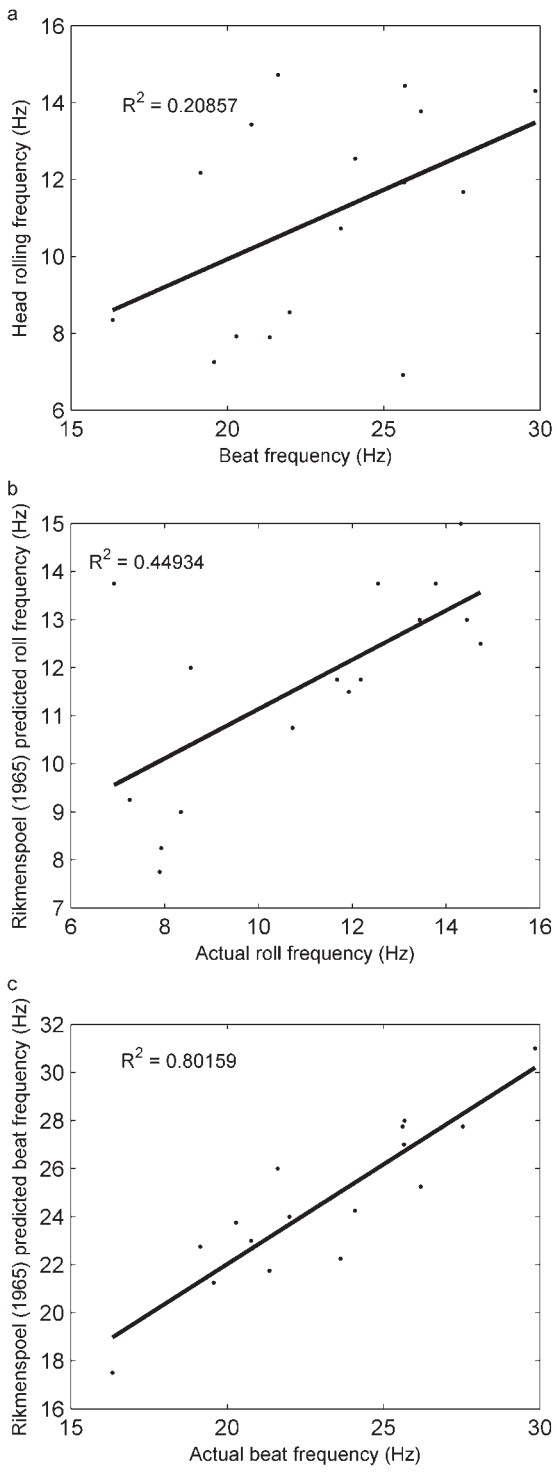

Fig. 4. Head rolling frequency and flagellar beat frequency in low viscosity liquid. (**a**) Actual flagellar beat frequency versus actual head rolling frequency. (**b**) Comparison between actual roll frequency measured from the head shape with the predicted roll frequency using the formula of Rikmenspoel (Eq. 2). (**c**) Comparison between actual flagellar frequency, with predicted flagellar frequency using the formula of Rikmenspoel (Eq. 3).

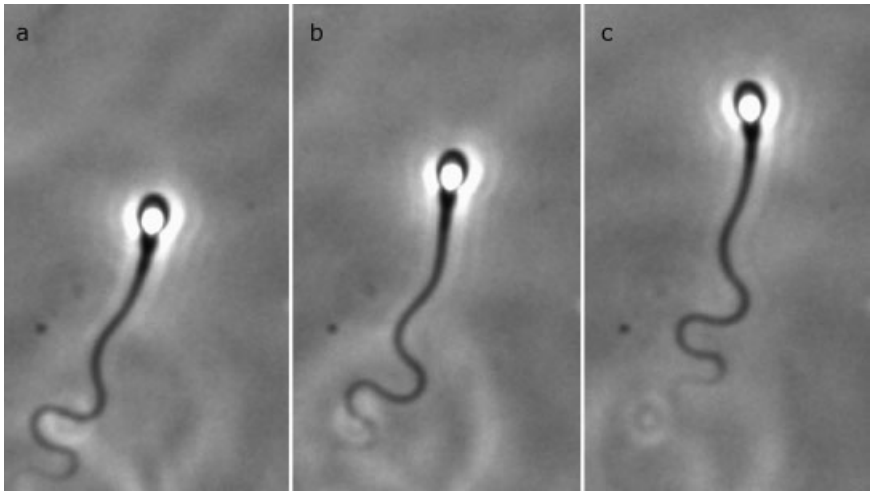

Fig. 5. A non-rolling cell in high viscosity liquid, shown at nominal frames 1, 40 and 100 (frame rate 332 Hz, total time interval between images **a** and **c** is 0.298 s).

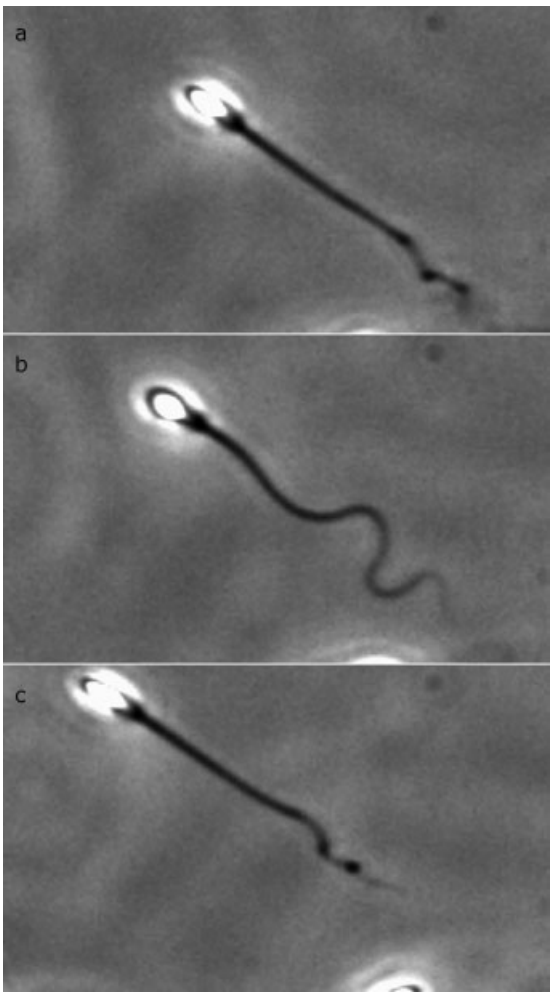

Fig. 6. A rolling cell in high viscosity liquid, shown at nominal frames 1, 40 and 100 (frame rate 332 Hz, total time interval between images **a** and **c** is 0.298 s).

one direction, cyan/blue indicates curvature in the other. Diagonal streaks depict the progression of bending waves along the flagellum, the slope of the streaks indicating wavespeed. The 'bumps' at the top of the plot indicate the variations in the projected flagellar length.

In the proximal 25 μm of the flagellum there is a clear 'yellow, cyan, cyan, yellow' pattern – for the implications of this see Discussion. A similar pattern was observed across the majority of cells observed in low viscosity liquid, although not all cells showed this pattern clearly. Additionally, due to rolling of the cell, some streaks change colour from blue to red or vice-versa, particularly near the end of the flagellum, as the rolling causes the apparent bending direction to reverse. In Fig. 7d, some repeated flagellar shapes are evident, as are high apparent curvatures near the flagellum tip, although it is also evident that the flagellum presents a wide array of shapes throughout the course of several beats, in clear contrast to the results shown later in Fig. 9d. Figure 7e shows the two frequency peaks in the head centreline deviation D, at 11.5 and 33.0 Hz, which are used in Eqs. 1 and 2 to predict the head rolling rate and actual flagellar beat frequency, analysed later in Fig. 11. A similar pair of frequency peaks was observed across all cells in low viscosity medium.

Artefacts in Images of Low Viscosity Rolling Motility

Figure 8 shows a selection of images of a typical cell in low viscosity liquid, a different example from that analysed in Fig. 7. These frames exhibit phenomena which are typical of imaging cells in low viscosity media (nominally movie frames 7, 16, 55 and 58, frame rate 332 Hz). Figures 8a and 8c show high 'apparent' curva-

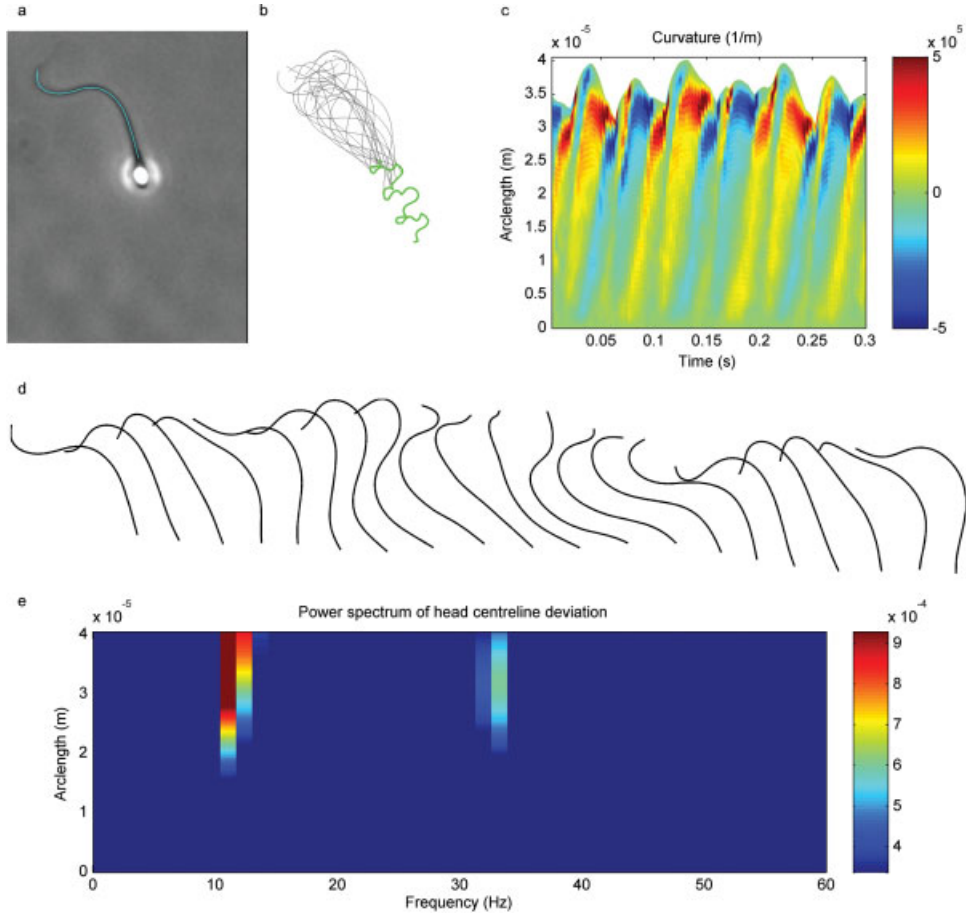

Fig. 7. Detailed analysis of a cell migrating in low viscosity liquid. (**a**) Example imaging frame, with the captured flagellar profile indicated in cyan. (**b**) Montage of flagellar positions (thin black lines, time interval 0.12 s) and the trajectory of the head/neck junction (green line, time interval 0.29 s). (**c**) Curvature portrait of flagellar movement as a function of time and arclength. (**d**) Montage of flagellar positions expanded from panel b. (**e**) Fourier power spectrum of head centerline deviation D, as defined in Fig. 2a, plotted for every position along the flagellum.

tures of the distal flagellum that may be due to out-of-plane movement, suggested by defocusing of certain regions of the flagellum. The apparent curvature calculated from a two-dimensional image may therefore be an over-estimate for the actual three-dimensional curvature. Figure 8b shows a flagellar profile in which the curvature is apparently relatively low; however there are two grey defocused segments separated by a black in-focus dot in the distal flagellum. This indicates out-of-plane bending waves that are not apparent or directly measurable in the two-dimensional projection. Figure 8d suggests the presence of torsion of the flagellum, indicated by successive bends appearing to be on the same 'side' to the viewer, a complication that was not observed in high viscosity liquids.

Analysis of the Flagellar Waveform: High Viscosity Liquid

Figure 9 assembles various detailed measures of the flagellar movement of a representative cell in high viscosity liquid. Figure 9a shows an example frame; see also Supporting Information Fig. 2 and Movie 2. A number of clear differences are evident comparing with the low viscosity example (Fig. 7). The path of the head/neck junction (Fig. 9b, green track) yaws very little, and does not exhibit such complex kinematic patterns, in particular being much more linear. Similar tracks were observed in all progressive cells analysed in high viscosity liquid. In the curvature plot (c), the lower beat frequency is evident from the reduced number of bending streaks, and their reduced gradient shows the slower wavespeed characteristic of high viscosity motility. Despite the superficial appearance of a 'steepening' wave in Figs. 9a and 9b, the wavelength and wavespeed are approximately constant along the length of the flagellum when calculated as a function of arclength. The maximum apparent curvatures are similar in high and low viscosity liquids, but high curvature values near to 6×10^5 m^{-1} are attained over much larger regions. Because of beat planarity, in high viscosity liquid the high curvatures

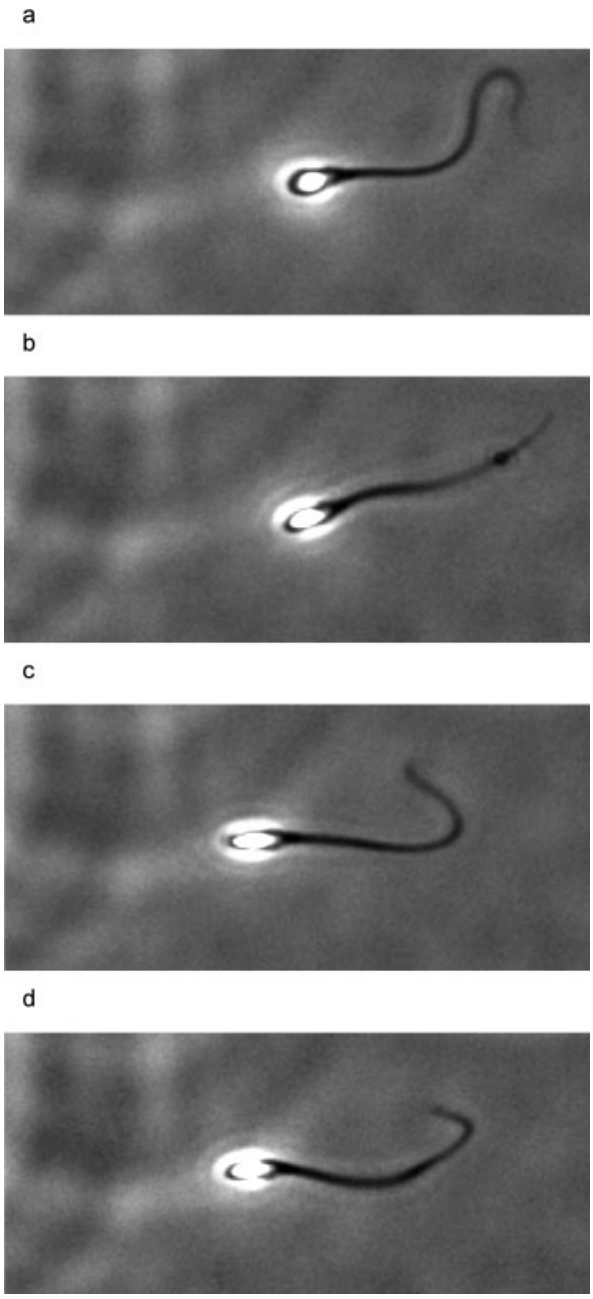

Fig. 8. A sequence of images of the same cell in low viscosity liquid, showing how the three-dimensional nature of the beat introduces artefacts. For qualitative analysis, see Results.

are genuine, and are not artefacts of projecting a three-dimensional wave onto a two-dimensional image plane. The curvature increases sharply around 20 μm from the head-midpiece junction, and the time-averaged absolute curvature is found to exhibit a nearly continuous increase, with a sharper gradient between 20 μm and 27 μm (Fig. 10, marked as 'A' and 'B'). Similar results were observed across other cells analysed.

Figure 9d shows the flagellar profile for comparison with Fig. 7d, and Fig. 9e shows the Fourier power spectrum of the cell in high viscosity liquid. Two peaks are evident, a relatively weak peak close to 3 Hz, and a stronger peak around 11 Hz, associated with the flagellar beat frequency.

Analysis of the Flagellar Waveform: Very High Viscosity Medium

A number of cells penetrating very high viscosity medium (2% methylcellulose) were also captured, these experiments being performed at 29°C. An example analysis for comparison with Figs. 7 and 9 is given in Fig. 11. The slower cell progression over a period of 0.34 s is evident (b) as is the slower progression of bending waves (c), but nevertheless there is considerable qualitative similarity in the beat pattern to the high viscosity (methylcellulose 1% solution) results in Fig. 9, although the wavelength is shortened further by the increased viscosity, resulting in up to three complete bending pairs being present on the flagellum instantaneously. Similar rolling and near-planar beating behaviour was observed in both high and very high viscosity liquids, although cells in very high viscosity liquid generally rolled more slowly, the typical example in Fig. 11 rolling at ~0.4 Hz.

DISCUSSION

The flagellar beat of human sperm in methycellulose mucus substitute was captured and reported in precise detail for the first time. The waveform was found to show great qualitative similarity to sketches and a micrograph of motile sperm in periovulatory cervical mucus [Katz et al., 1978; Gaddum-Rosse et al., 1980], our imaging and analysis now showing in quantitative detail how the wave develops and progresses along the flagellum. This is the first study to employ high frame rate digital imaging of the migrating cohort of human sperm in liquids with viscosity approximating periovulatory cervical conditions.

Flagellar Kinematics and Their Effect on Progressive Velocity

While there were considerable differences in the wavespeeds, wavelengths and frequencies of cells in low and high viscosities, the mean progressive velocities were similar, being 62 μm/s and 65 μm/s respectively ($n = 16$ and $n = 19$). The correlations observed in low viscosity were consistent with the characteristic linear dependence on wavespeed and wavelength expected from fluid mechanics models and reported previously, however the results for high viscosity did not show clear correlations. This may be due to non-Newtonian effects, or it may be due to the fact that previous theoretical studies

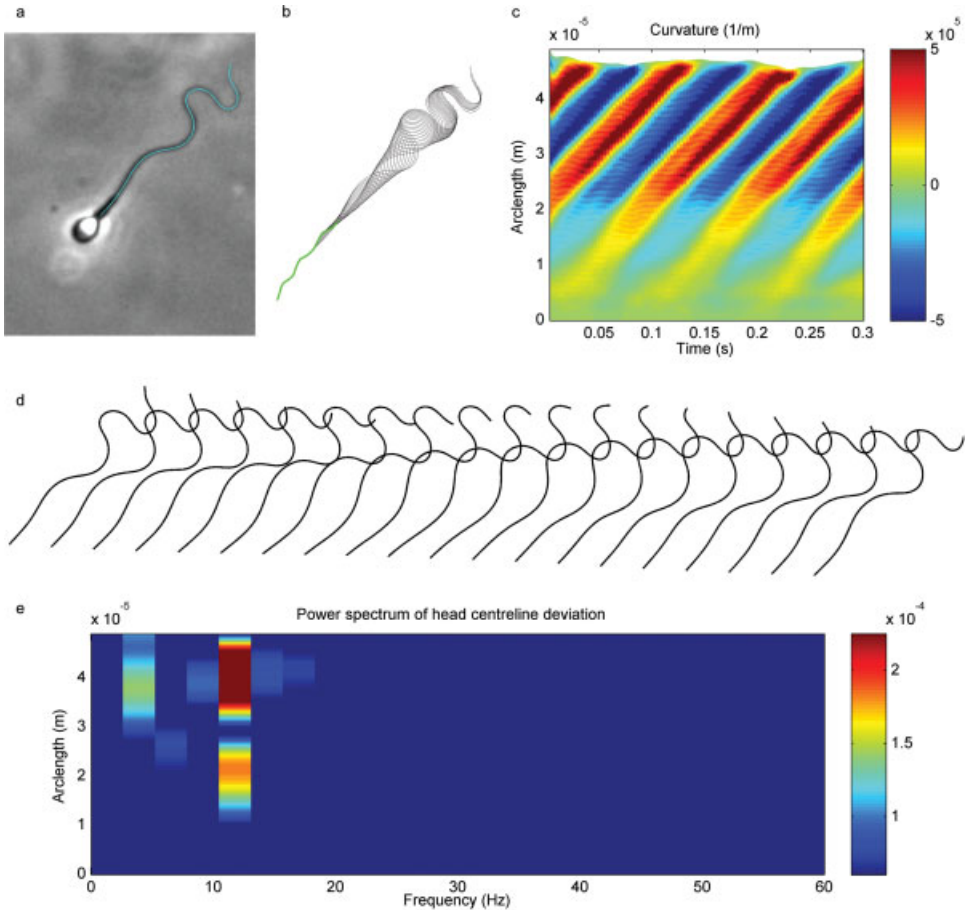

Fig. 9. Detailed analysis of a non-rolling cell migrating in high viscosity liquid; for detailed explanation see the caption of Fig. 7 and Results text.

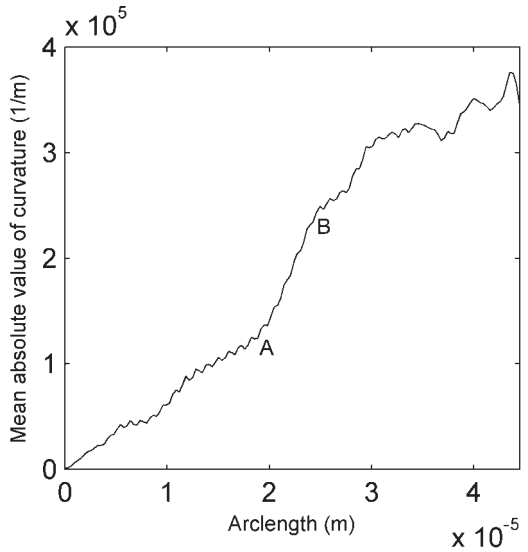

Fig. 10. Mean absolute value of curvature as a function of distance along the flagellum for the cell in high viscosity liquid analysed in detail in Fig. 9. The points 'A' and 'B' denote the region of the flagellum where the mean absolute curvature increases most rapidly as a function of arclength.

systematically examining the relation between kinematic parameters and swimming velocity have not generally included fluid-structure-internal mechanics interaction. This interaction is clearly very important in high viscosity liquids where the viscous load on the flagellum induces changes to the waveform. Our results differed somewhat from an early study of sperm penetrating a relatively short distance into cervical mucus [Katz et al., 1978], in which positive correlations were observed. A possible explanation is that our sample was more homogeneous in progressive velocity (range 34 μm/s) than the earlier study (range ~60 μm/s), likely due to our selection of cells that had migrated 2 cm. Another early study using cervical mucus and a migration assay [Katz et al., 1982] reported a correlation between ln(frequency) and ln(velocity), with progressive velocity being approximately proportional to the square root of frequency, provided that 'vanguard' and 'following' cells were analysed separately. Scatter plots of the results and associated correlation coefficients were not given, however they did report a statistically significant correlation,

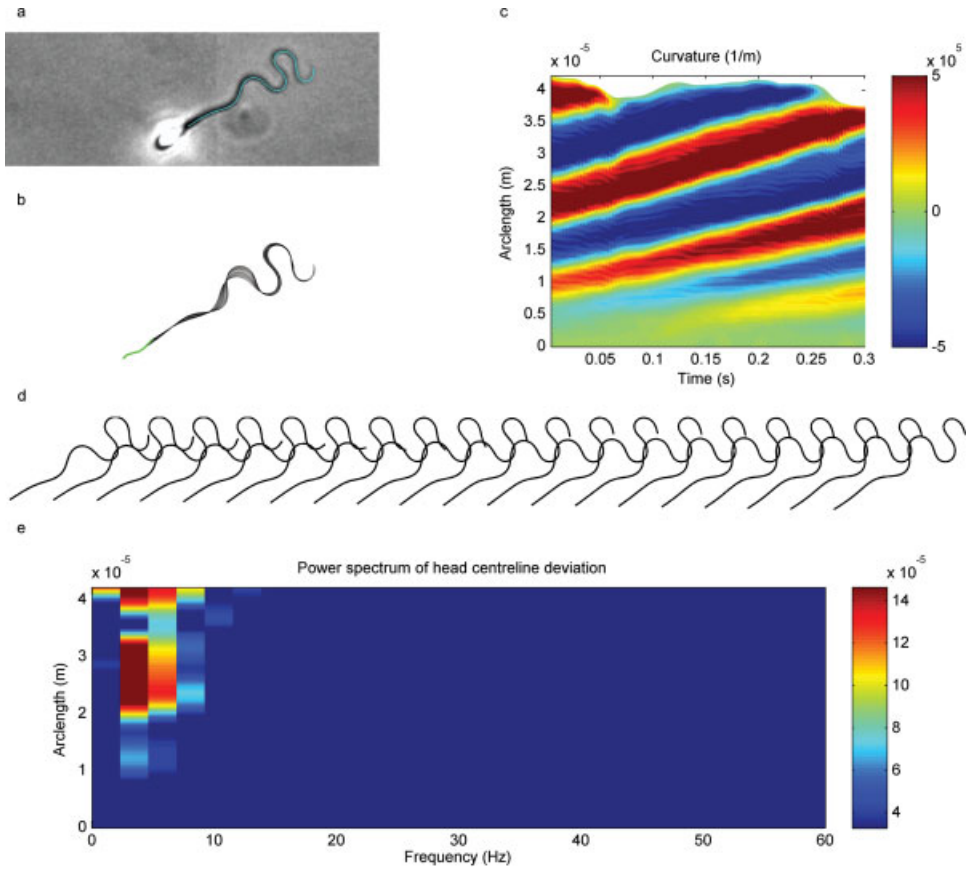

Fig. 11. Detailed analysis of a rolling cell migrating in 'very high viscosity liquid' (methylcellulose 2%), for explanation see Fig. 7 caption and Results text.

suggesting that modification of the liquid medium by migrating cells may be an additional complicating factor. Intriguingly, the 34 μm/s range in progressive velocity of cells in high viscosity liquid we observed was not explained by the kinematic parameters.

Analysing the average distance progressed by cells per flagellar beat, we found that in both liquids progression per beat was proportional to wavelength; however the slope of the relationship was very different. Despite the fact that in high viscosity liquid the average wavelength was smaller, the mean progression per beat was 5.3 μm, compared with a mean value of 2.7 μm in low viscosity.

The power spectra shown in Figs. 7e and 9e justify that the beat pattern can be represented to a good approximation by a sinusoidal oscillation. Under this approximation, we have the following relation:

$$\text{Wavespeed} = \text{frequency} \times \text{wavelength}. \qquad (3)$$

Wavespeed was found to vary only by a relatively small factor (around 35%) in high viscosity medium, suggesting that liquid viscosity constrains the speed at which bending waves may progress. Hence if wavespeed is constrained, an increase in wavelength, which in high viscosity medium will increase the progression per beat, will typically be accompanied by a reduction in frequency. This will result in fewer beats being performed per second, negating any significant propulsive advantage. Conversely, a 'beneficial' increase in frequency will be accompanied by a 'detrimental' decrease in wavelength, giving some insight into the apparent lack of a clear correlation between parameters such as frequency and wavelength, and progressive velocity in high viscosity liquids.

Frequency may be an important factor in distinguishing the very first cells – the 'vanguard' – to migrate through mucus, as indicated by the early Kremer assay study [Katz et al., 1982]. Frequency may also distinguish cells which migrate long distances as opposed to those which merely penetrate a short distance, indicated by the early study which interfaced mucus and semen [Katz et al., 1978].

Cell Rolling and Flagellar Torsion

Theoretical models show that cell rolling occurs because of non-planarity of the flagellar beat and the

effect of torque balance between the head and flagellum [Chwang and Wu, 1971]. A cell with a fully helical waveform will roll most rapidly, a cell with a 'flattened helicoid' waveform will roll more slowly, and a cell with an almost planar beat will roll more slowly still. Because the human sperm head is relatively compact, the torque balance effect means that even a modestly non-planar beat will cause rolling at a similar rate to the flagellar beat. The relatively high rolling rate of cells in low viscosity medium implies the existence of non-planar components, confirmed by the fact that in the low viscosity images, at no point did the waveform appear 'sideways on', as was observed in high viscosity.

In low viscosity imaging we observed that two-dimensional apparent flagellum length varies with a similar frequency to the rolling of the head, implying that the three-dimensional flagellar 'envelope' rotates at a similar rate to the head. This is consistent with early models of free-swimming bull sperm [Rikmenspoel, 1965] and observations of tethered human sperm [Ishijima et al., 1986] which described the flagellar beat envelope as an 'elliptical cone'.

Perhaps surprisingly, the head-rolling rate was found only to be weakly correlated with flagellar beat frequency. This shows that the flagellar beat does not produce the same rotation angle in every cell, and hence that the torque induced by non-planarity of the flagellar beat far from being homogeneous across all cells. The mean angle of rotation of the head per flagellar beat was 172°, close to the approximate value of 180° reported in an early study [Phillips, 1972]. Rolling of the cell affects the way that the alternating bending pattern of the flagellum with respect to head appears to the stationary observer. The curvature analysis (Fig. 7c) shows a yellow, cyan, cyan, yellow sequence of diagonal stripes, which we interpret as arising from a 'left, right, left, right' bending pattern with respect to the cell, modified by the cell rolling ~180° between the first 'left' bend and the second 'left' bend.

Ishijima et al. [1986, 1992] reported similar rolling frequencies to our study (mean values of 9–11 Hz respectively) but lower flagellar frequencies (mean ~11 Hz), suggesting a rolling rate of ~360° per flagellar beat cycle. This significant difference may be due to the differing experimental conditions: the study of Ishijima et al. used tethered cells for the measurement of beat frequency rather than free-swimming cells. If free-swimming sperm were to roll a full 360° with each alternating bending pair, then the cell would roll 180° with each bend. Hence every bend would appear to the observer as being on the same 'side', resulting in all of the stripes on the curvature plot being the same colour. Indeed we have observed such an effect occurring in hyperactivated cells in low viscosity liquid, constrained by a shallow imaging chamber (Smith et al., unpublished data).

We found that the two-dimensional imaging data exhibit two characteristic frequencies in low viscosity liquid that can be explained by the combined effect of the flagellar beat frequency and the rolling rate. We found that the beat frequency was predicted with reasonable accuracy from the Fourier frequency peaks by the model of Rikmenspoel [1965], but that the prediction of rolling rate was not as precise, possibly due to the fact that the rolling rate of the head is not constant. We additionally found evidence confirming the existence of significant torsion in the flagella of free-swimming human sperm cells in low viscosity liquids, a feature that was not evident in high viscosity. Active interbend torsion has been reported from observations of several other mammalian species' sperm [Woolley, 2003].

In high viscosity liquid, both rolling and non-rolling cells were observed, and even in very high viscosity (methylcellulose 2%) solution, cells were still observed to roll, with a typical rate being ~1.5 Hz. Cells viewed side-on revealed a nearly planar beat, which has previously been observed in tethered cells [Ishijima et al., 1986], again emphasising that experimental studies of flagellar function and clinical diagnostics performed in low viscosity liquids may induce the flagellum to behave in a way that is not physiological.

The 'High Viscosity' Waveform and Human Sperm Flagellar Ultrastructure

Detailed analysis showed that, despite superficial appearance, wavespeed and wavelength, measured as functions of arclength were found to be approximately constant along the flagellum at high viscosity, as reported for bull sperm [Rikmenspoel, 1984]. The high viscosity waveform arises from a combination of near-constant propagation speed and a continuous increase in curvature as the wave propagates. The latter feature does not appear to occur at any viscosity in sea urchin sperm [Woolley and Vernon, 2001], the chief evolutionary difference in such cells being the absence of accessory structures such as the outer dense fibres and fibrous sheath. It has previously been suggested that differences between mammalian and marine species' sperm may in part be due to these accessory structures [Lindemann, 1996]. An early modelling and imaging study of the bull sperm flagellum has shown that some of the features of the high viscosity waveform are predicted by a model that has linearly decreasing stiffness along the principal piece [Rikmenspoel, 1984].

Sea urchin sperm respond differently to high viscosity, and in particular, at 1.5 Pa·s fully 'helical' flagellar beating may occur [Woolley and Vernon, 2001]. Since free-swimming cells with highly compacted heads

such as human sperm cannot progress effectively under the action of a true helical wave, there must have evolved a mechanism to prevent fully helical beating from occurring in vivo in high viscosity liquids. The fibrous sheath of mammalian sperm contains two relatively thick longitudinal columns, associated with doublets 3 and 8 of the axoneme [Fawcett, 1975] that, acting together with a viscous loading may constrain the flagellum to a planar beat [Lindemann, 1996].

Curvature is developed through a balance of dynein activity causing microtubule sliding, elastic stiffness of the flagellum and viscous forces resisting motion of the flagellum through the fluid [Brokaw, 1966]. The fibrous sheath gradually thins along the length of the principal piece [Fawcett, 1975], with outer dense fibres 3 and 8 terminating 6 μm along the principal piece, fibres 4, 2, 7 terminating 17–21 μm along the principal piece and fibres 5, 6, 9 and 1 terminating 31–35 μm along the principal piece [Serres et al., 1983]. This likely reduces the elastic stiffness and potentially results in the increasing curvatures attained along the flagellum in the presence of high viscosity and hence the characteristic beat shape. Biophysical modelling may help to explain how this characteristic shape results in efficient and effective progression.

In very high viscosities produced from solutions of methylcellulose 2% (nominal viscosity 4 Pa·s at 20°C, although we performed these experiments at 29°C), we observed (Fig. 11) a waveform that did not differ qualitatively from that observed in 1% solutions. Studies of sea urchin [Woolley and Vernon, 2001] and quail sperm [Woolley, 2007] in such liquids report extreme coiling of the flagellum and a flagellar wave that remarkably does not appear to move with respect to the observer. Again, the stiffening effect of the fibrous sheath is likely to be responsible for this difference.

Mathematical modelling has suggested that the outer dense fibres allow mammalian sperm flagella to adapt to higher viscous loads by essentially 'running in a lower gear' [Lindemann, 1996], with dynein arm force transferred from microtubules to the outer dense fibres, effectively increasing the 'lever arm' distance, providing a mechanical advantage, and additionally engaging more dynein molecules per bend. This would result in a greater bending moment at the cost of a lower sliding velocity, allowing mammalian sperm to maintain effective motility over several orders of magnitude increase in viscous resistance.

Liquids containing 2% methylcellulose may prove to be informative experimental models for physiological liquids having much higher viscosity than periovulatory cervical mucus. Examples include the higher viscosity, less hydrated mucus occurring at other points in the cycle [Wolf et al., 1977] or under the action of oral contraceptives [Wolf et al., 1979], mucus which may occlude the isthmus [Jansen, 1980] or the viscoelastic environment of the cumulus-oocyte complex [Drobnis et al., 1988].

CONCLUSIONS

To summarise, viscosity significantly alters rolling rate, planarity, torsion, waveform, trajectory and progression per beat, although not progressive velocity. The scaling laws relating kinematic parameters to progression are very different in low and high viscosities, and in particular there appears to be a constraint on the wavespeeds that may be attained in high viscosity liquids. Hence observations of cells in low viscosity liquids may be uninformative regarding motility in vivo.

A consequence of the reduced rolling rate and increased planarity in high viscosity is that the full waveform may be captured accurately for a period of several or many beats, which is expedient for the assessment of flagellar movement with two-dimensional techniques. More sophisticated techniques such as two-colour darkfield 'defocusing' microscopy are required to give quantitative information for cells that have fully three-dimensional flagellar beats [Woolley, 1981], and automated analysis of these images may prove more challenging. Due to the steady progression of the bending wave, the relatively high frame rates employed may not be necessary to capture important biophysical properties of the waveform – although some 'oversampling' reduces the impact of noise.

For these reasons, research assessing human sperm motility and its chemical modulation should employ, at least in part, the use of physiological high viscosity liquids in order to have relevance to natural conception. Nevertheless, consideration of the biophysics of low viscosity motility may still be important in understanding the function and possible modulation of sperm in standard IVF, and possibly in follicular fluid around the time of ovulation.

Solution containing 1% methylcellulose was found in oscillatory rheometry to give similar order-of-magnitude effective viscosity to periovulatory mucus, although with shorter relaxation time. The relaxation time of cervical mucus can be estimated to be ~0.03 s from previous studies, which is a similar order of magnitude to the duration of the flagellar beat, and so may be important in vivo. This may be an important effect to take into account in future studies, for example through the use of long chain polyacrylamide [Suarez and Dai, 1992], or through the use of varying mixtures of hydroxypropylmethylcellulose and sodium carboxymethylcellulose [Alvarez-Lorenzo et al., 2001], allowing the modulation of both storage and loss modulus and hence testing of

the effect of each of these rheological properties on the flagellar beat and motility separately.

In the flagella of caput and caudal spermatozoa of the selenoprotein $P^{-/-}$ knockout mouse [Olson et al., 2005], disruption of the outer dense fibres and the mitochondrial sheath near to the annulus are associated with the formation of a 'hairpin' bend in the disrupted region. A similar effect is observed in Septin 4 null mice [Kissel et al., 2005]; Septin 12 also being likely to be crucial to annulus formation [Steels et al., 2007]. The loss of the mechanical stiffness in this region may be the cause of this defect, although it is unclear whether this is caused by loss of mitochondria, disruption of the dense fibres or a combination of these factors – clearly there is an important role for biophysical modelling in the interpretation of such observations. Unrelated observations on 'normal' human sperm adhered to surfaces reveal that when intracellular calcium is artificially elevated in this region via treatment with 4-aminopyridine, marked bending can even occur in the proximal flagellum [Fig. 5b, Bedu-Addo et al., 2008]; similar treatment of free-swimming cells is known to induce hyperactivation [Gu et al., 2004]. Our results show that advanced biophysical models of flagellar movement are required, and these will be critical to interpreting biomedical studies of motility and its regulation, for example in determining energy requirements in different regions of the flagellum, which are necessary in elucidating the role of different ATP transport pathways [Ford, 2006], in interpreting the hyperactivated state and how it may result in different motility patterns in physiological liquids [Suarez and Dai, 1992; Ho and Suarez, 2001], and in linking receptor biology and signalling to mechanics and behaviour in human sperm chemotaxis [Eisenbach, 2007]. This work will be essential to understanding novel modulators of sperm motility and hypotheses regarding chemotaxis and other forms of motility modulation.

ACKNOWLEDGMENTS

The authors thank members of the Reproductive Biology and Genetics group, University of Birmingham; staff at the Assisted Conception Unit, Birmingham Women's Hospital; Professor John Blake, School of Mathematics, University of Birmingham; Dr. Stephen Publicover, School of Biosciences, University of Birmingham; and Mr. Henry Shum, Mathematical Institute, University of Oxford, for valuable discussions. The authors also acknowledge insightful comments from the anonymous referees.

REFERENCES

Aitken RJ, Bowie H, Buckingham D, Harkiss D, Richardson DW, West KM. 1992. Sperm penetration into a hyaluronic acid polymer as a means of monitoring functional competance. J Androl 13:44–54.

Alvarez-Lorenzo C, Duro R, Gomez-Amoza JL, Martinez-Pacheco R, Souto C, Concheiro A. 2001. Influence of polymer structure on the rheological behaviour of hydroxypropyl-methylcellulose-sodium carboxymethylcellulose dispersions. Colloid Polym Sci 279:1045–1057.

Barratt CLR, Osborn JC, Harrison PE, Monks N, Dunphy BC, Lenton EA, Cooke ID. 1989. The hypo-osmotic swelling test and the sperm mucus penetration test in determining fertilization of the human oocyte. Hum Reprod 4:430–434.

Bedu-Addo K, Costello S, Harper C, Machado-Oliveira G, Lefievre L, Ford C, Barratt C, Publicover S. 2008. Mobilisation of stored calcium in the neck region of human sperm – A mechanism for regulation of flagellar activity. Int J Dev Biol 52:615–626.

Bohmer M, Van Q, Weyand I, Hagen V, Beyermann M, Matsumoto M, Hoshi M, Hildebrand E, Kaupp UB. 2005. Ca^{2+} spikes in the flagellum control chemotactic behaviour of sperm. EMBO J 24:2741–2752.

Brokaw CJ. 1966. Bend propagation along flagella. Nature 209:161–163.

Chwang AT, Wu TY. 1971. Helical movement of micro-organisms. Proc Royal Soc London Series B: Biol Sci 178:327–346.

Denehy MA. 1975. Propulsion of nonrotating ram and oyster spermatozoa. Biol Reprod 13:17–29.

Dresdner RD, Katz DF. 1981. Relationships of mammalian sperm motility and morphology to hydrodynamic aspect of cell function. Biol Reprod 25:920–930.

Drobnis EZ, Yudin AI, Cherr GN, Katz DF. 1988. Kinematics of hamster sperm during penetration of the cumulus cell matrix. Gamete Res 21:367–383.

Eisenbach M. 2007. A Hitchhiker's guide through advances and conceptual changes in chemotaxis. J Cell Physiol 213:574–580.

Eisenbach M, Giojalas LC. 2006. Sperm guidance in mammals – An unpaved road to the egg. Nat Rev Mol Cell Biol 7:276–285.

Fawcett DW. 1975. The mammalian spermatozoon. Devel Biol 44:394–436.

Ford WCL. 2006. Glycolysis and sperm motility: Does a spoonful of sugar help the flagellum go round? Hum Reprod Update 12:269–274.

Gaddum-Rosse P, Blandau RJ, Lee WI. 1980. Sperm penetration into cervical-mucus in vitro. I. Comparative studies. Fertil Steril 33:636–643.

Gray J. 1953. Undulatory propulsion. Q J Microsc Sci 94:551–578.

Gray J. 1955. The movement of sea-urchin spermatozoa. J Exp Biol 32:775–800.

Gray J, Hancock GJ. 1955. The propulsion of sea-urchin spermatozoa. J Exp Biol 32:802–814.

Gu Y, Kirkman-Brown JC, Korchev Y, Barratt CLR, Publicover SJ. 2004. Multi-state, 4-aminopyridine-sensitive ion channels in human spermatozoa. Dev Biol 274:308–317.

Ho HC, Suarez SS. 2001. Hyperactivation of mammalian spermatozoa: Function and regulation. Reproduction 122:519–526.

Ishijima S, Oshio S, Mohri H. 1986. Flagellar movement of human spermatozoa. Gamete Res 13:185–197.

Ishijima S, Hamaguchi MS, Naruse M, Ishijima SA, Hamaguchi Y. 1992. Rotational movement of a spermatozoon around its long axis. J Exp Biol 163:15–31.

Ishijima S, Baba SA, Mohri H, Suarez SS. 2002. Quantitative analysis of flagellar movement in hyperactivated and acrosome-reacted golden hamster spermatozoa. Mol Reprod Dev 61:376–384.

Ishijima S, Mohri H, Overstreet JW, Yudin AI. 2006. Hyperactivation of monkey spermatozoa is triggered by Ca^{2+} and completed by cAMP. Mol Reprod Dev 73:1129–1139.

Ivic A, Onyeaka H, Girling A, Brewis IA, Ola B, Hammadieh N, Papaioannou S, Barratt CLR. 2002. Critical evaluation of methylcellulose as an alternative medium in sperm migration tests. Hum Reprod 17:143–149.

Jansen RPS. 1980. Cyclic changes in the human fallopian tube isthmus and their functional importance. Am J Obstet Gynaecol 136:292–308.

Kaneko T, Mori T, Ishijima S. 2007. Digital image analysis of the flagellar beat of activated and hyperactivated suncus spermatozoa. Mol Reprod Dev 74:478–485.

Katz DF, Berger SA. 1980. Flagellar propulsion of human sperm in cervical mucus. Biorheology 17:169–175.

Katz DF, Mills RN, Pritchett TR. 1978. The movement of human spermatozoa in cervical mucus. J Reprod Fertil 53:259–265.

Katz DF, Overstreet JW, Hanson FW. 1980. A new quantitative test for sperm penetration into cervical mucus. Fertil Steril 33:179–186.

Katz DF, Brofeldt BT, Overstreet JW, Hanson FW. 1982. Alteration of cervical mucus by vanguard human spermatozoa. J Reprod Fertil 65:171–175.

Kinukawa M, Oda S, Shirakura Y, Okabe M, Ohmuro J, Baba SA, Nagata M, Aoki F. 2006. Roles of cAMP in regulating microtubule sliding and flagellar bending in demembranated hamster spermatozoa. Febs Lett 580:1515–1520.

Kissel H, Georgescu MM, Larisch S, Manova K, Hunnicutt GR, Steller H. 2005. The Sept4 septin locus is required for sperm terminal differentiation in mice. Dev Cell 8:353–364.

Kremer J. 1965. A simple sperm penetration test. Int J Fertil 10:209–215.

Lindemann CB. 1996. Functional significance of the outer dense fibers of mammalian sperm examined by computer simulations with the geometric clutch model. Cell Motil Cytoskeleton 34:258–270.

Mortimer D, Mortimer ST, Shu MA, Swart R. 1990. A simplified approach to sperm-cervical mucus interaction testing using a hyaluronate migration test. Hum Reprod 5:835–841.

Nishigaki T, Wood CD, Tatsu Y, Yumoto N, Furuta T, Elias D, Shiba K, Baba SA, Darszon A. 2004. A sea urchin egg jelly peptide induces a cGMP-mediated decrease in sperm intracellular Ca^{2+} before its increase. Dev Biol 272:376–388.

Ohmuro J, Ishijima S. 2006. Hyperactivation is the mode conversion from constant-curvature beating to constant-frequency beating under a constant rate of microtubule sliding. Mol Reprod Dev 73:1412–1421.

Ohmuro J, Mogami Y, Baba SA. 2004. Progression of flagellar stages during artificially delayed motility initiation in sea urchin sperm. Zool Sci 21:1099–1108.

Ola B, Afnan M, Papioannou S, Sharif K, Bjorndahl L, Coomarasamy A. 2003. Accuracy of sperm-cervical mucus penetration tests in evaluating sperm motility in semen: A systematic quantitative review. Hum Reprod 18:1037–1046.

Olson GE, Winfrey VP, Nagdas SK, Hill KE, Burk RF. 2005. Selenoprotein P is required for mouse sperm development. Biol Reprod 73:201–211.

Phillips DM. 1972. Comparative analysis of mammalian sperm motility. J Cell Biol 53:561–573.

Rikmenspoel R. 1965. The tail movement of bull spermatozoa. Observations and model calculations. Biophys J 5:365–392.

Rikmenspoel R. 1984. Movements and active moments of bull sperm flagella as a function of temperature and viscosity. J Exp Biol 108:205–230.

Serres C, Escalier D, David G. 1983. Ultrastructural morphometry of the human-sperm flagellum with a stereological analysis of the lengths of the dense fibers. Biol Cell 49:153–162.

Shiba K, Ohmuro J, Mogami Y, Nishigaki T, Wood CD, Darszon A, Tatsu Y, Yumoto N, Baba SA. 2005. Sperm-activating peptide induces asymmetric flagellar bending in sea urchin sperm. Zool Sci 22:293–299.

Shiba K, Tagata T, Ohmuro J, Mogami Y, Matsumoto M, Hoshi M, Baba SA. 2006. Peptide-induced hyperactivation-like vigorous flagellar movement in starfish sperm. Zygote 14:23–32.

Smith DJ, Gaffney EA, Blake JR. 2007. A viscoelastic traction layer model of muco-ciliary transport. Bull Math Biol 69:289–327.

Spehr M, Gisselmann G, Poplawski A, Riffell JA, Wetzel CH, Zimmer RK, Hatt H. 2003. Identification of a testicular odorant receptor mediating human sperm chemotaxis. Science 299:2054–2058.

Spehr M, Schwane K, Riffell JA, Zimmer RK, Hatt H. 2006. Odorant receptors and olfactory-like signaling mechanisms in mammalian sperm. Mol Cell Endocrinol 250:128–136.

Steels JD, Estey MR, Froese CD, Reynaud D, Pace-Asciak C, Trimble WS. 2007. Sept12 is a component of the mammalian sperm tail annulus. Cell Motil Cytoskel 64:794–807.

Suarez SS, Dai XB. 1992. Hyperactivation enhances mouse sperm capacity for penetrating viscoelastic media. Biol Reprod 46:686–691.

Suarez SS, Ho HC. 2003. Hyperactivation of mammalian sperm. Cell Mol Biol (Noisy-le-grand) 49:351–356.

Teves ME, Barbano F, Guidobaldi HA, Sanchez R, Miska W, Giojalas LC. 2006. Progesterone at the picomolar range is a chemoattractant for mammalian spermatozoa. Fertil Steril 86:745–749.

Ward GE, Brokaw CJ, Garbers DL, Vacquier VD. 1985. Chemotaxis of *Arbacia punctulata* spermatozoa to resact, a peptide from the egg jelly layer. J Cell Biol 101:2324–2329.

Wolf DP, Blasco L, Khan MA, Litt M. 1977. Human cervical mucus. II. Changes in viscoelasticity during the menstral cycle. Fertil Steril 28:47–52.

Wolf DP, Blasco L, Khan MA, Litt M. 1979. Human cervical-mucus. V. Oral-contraceptives and mucus rheologic properties. Fertil Steril 32:166–169.

Wood CD, Darszon A, Whitaker M. 2003. Speract induces calcium oscillations in the sperm tail. J Cell Biol 161:89–101.

Wood CD, Nishigaki T, Tatsu Y, Yumoto N, Baba SA, Whitaker M, Darszon A. 2007. Altering the speract-induced ion permeability changes that generate flagellar Ca^{2+} spikes regulates their kinetics and sea urchin sperm motility. Dev Biol 306:525–537.

Woolley DM. 1981. A method for determining the three-dimensional form of active flagella, using two-colour darkground illumination. J Microsc 121:241–244.

Woolley DM. 2003. Motility of spermatozoa at surfaces. Reproduction 126:259–270.

Woolley DM. 2007. A novel motility pattern in quail spermatozoa with implications for the mechanism of flagellar beating. Biol Cell 99:663–675.

Woolley DM, Vernon GG. 2001. A study of helical and planar waves on sea urchin sperm flagella, with a theory of how they are generated. J Exp Biol 204:1333–1345.

APPENDIX

Glossary of Biophysical Terminology

Viscoelasticity: A material property denoting a combination of both viscous and elastic behaviour upon material deformation.

Viscoelastic fluid: A material which will deform continuously under a constant applied stress (force per

unit area), as with a viscous fluid, and which additionally exhibits elastic properties. Mucus is an important biological example. Viscoelastic fluid properties are measured using techniques such as oscillatory rheometry.

Relaxation time: The time period characterising the response of a *viscoelastic* material. In particular when a *viscoelastic fluid* such as mucus is deformed and released for a time period significantly shorter than the relaxation time, the material will behave as an elastic solid, recoiling to its initial configuration without dissipating energy. When deformed for periods significantly longer than the relaxation time, a *viscoelastic fluid* will behave as a viscous liquid, dissipating energy.

Rheology: The flow properties of a material. On microscopic scales, liquids that do not contain polymer, such as saline media, have simple flow '*Newtonian*' properties characterised by a single constant parameter, the viscosity. More complex rheologic properties resulting from polymeric concentrations include viscoelasticity and shear-thinning.

Shear rate: The flow velocity gradient, i.e. the rate at which layers of fluid flow over each other, quantified in inverse seconds, typically being proportional to flagellar beat frequency.

Shear-thinning: The property of a liquid becoming less viscous at high rates of shear.

Storage modulus: A parameter characterising the elastic behaviour of a viscoelastic material at a given frequency, measured in Pascals (Newtons per square metre). A Newtonian liquid such as saline has storage modulus approximately zero.

Loss modulus: A parameter characterising the viscous behaviour of a viscoelastic material at a given frequency, measured in Pascal. A Newtonian liquid such as saline has loss modulus approximately equal to its velocity multiplied by its frequency, multiplied by 6.28.

Maxwell liquid: A simple physical model of a *viscoelastic fluid*, characterised by a viscosity and a *viscoelastic fluid relaxation time*, or equivalently *storage* and *loss moduli*. The Maxwell liquid can be conceptualised as consisting of fluid volumes behaving as dashpot-spring series.

Glossary of Sperm Motility Terminology

Progressive motility: Forwards motion of the cell, considered to be essential for migration through the female reproductive tract to the site of fertilisation.

Hyperactivated motility: Non-progressive motility characterised by high flagellar curvature and asymmetric beating, speculated to be essential for sperm penetration of the layers surrounding the egg.

Beat cycle: The production and propagation along the flagellum of an alternating pair of bends.

Progressive velocity: The velocity at which a cell moves in its overall direction of motion, an important indicator of fertilising potential.

Progression per beat: The distance moved by a cell over the course of a beat cycle, equal to the progressive velocity divided by the beat frequency.

Flagellar arclength: Distance along the curved flagellum, measured from the head/midpiece junction. This can be visualised as the length of a piece of string following the flagellum.

Wavelength: The arclength distance covering a bending pair

Wavespeed: The rate at which a bend moves, measured from flagellar arclength, equal to the wavelength multiplied by the frequency.

Planarity: The extent to which the flagellum moves in a plane, typically coinciding with the plane-of-flattening of the head.

Torsion: Twisting of the flagellum about its central axis. The central axis can be visualised as the inner doublet microtubules.